

Crystal Sizes and Energy Gaps of Cerium Oxide Using Co-Precipitation Method

Paochi Chen

Lunghwa University of Science and Technology, Taiwan

Email: chenpc@mail2000.com.tw

How to cite this paper: Chen, P.C. (2022) Crystal Sizes and Energy Gaps of Cerium Oxide Using Co-Precipitation Method. *Materials Sciences and Applications*, 13, 213-231.

<https://doi.org/10.4236/msa.2022.134012>

Received: March 11, 2022

Accepted: April 26, 2022

Published: April 29, 2022

Copyright © 2022 by author(s) and Scientific Research Publishing Inc. This work is licensed under the Creative Commons Attribution International License (CC BY 4.0).

<http://creativecommons.org/licenses/by/4.0/>



Open Access

Abstract

Co-precipitation was used to prepare cerium oxide nano-particles. The effects of aging temperature and concentration of cobalt ion on the optical property, morphology, and particle size were investigated. The cerium oxide was prepared by adding ammonia solution into a mixed solution of cerium nitrate with cobalt nitrate solutions to obtain a large amount of precipitates and then aged further. Subsequently, the precipitates were kept in an oven for calcination keeping the temperature at 400°C for lasting 24 h. The average size of cerium oxide particles was obtained from the (111) peak in the X-ray diffraction pattern using the Scherrer equation. The crystal sizes obtained were found to be in the range of 11.82 - 13.47 nm. The results showed that the particle size decreased with an increase in the Co ion concentration and decreased with an increase in temperature. The SEM pictures show that the morphology for cerium oxide is granular and/or columnar. It can be seen from UV/Vis absorption spectrum that the maximum absorption peaks were in the range of 334 - 390 nm, depending on the operating conditions. The corresponding energy gaps were observed in the range of 3.18 - 3.71 eV. Subsequently, the Brus equation for the energy gap was discussed. Finally, particle size was correlated with the aging temperature and Co ion concentration.

Keywords

Co-Precipitation, Hydrothermal Method, Cerium Oxide, Energy Gap

1. Introduction

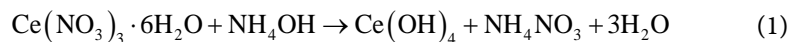
The metal oxides, such as TiO₂, CeO₂, ZrO₂, SiO₂, Al₂O₃, and ZnO, play a considerably leading part in the domains of material, physics, and chemistry and have been extensively used in industrial processes and materials, such as catalyst, fuel cell, piezoelectric material, sensor material, and optical component [1]. Among

various metal oxides, CeO₂ is one of the extensively discussed and applied metal oxides. CeO₂ has a face-centered cubic structure with a high melting point (2400°C - 2700°C) [2] [3] and is nonflammable and insoluble in solvents of dilute acid, ethanol, and water. A remarkable property of CeO₂ is the number of effective redox Ce³⁺/Ce⁴⁺ sites and their ability to exchange oxygen [2]. Therefore, it has good optical properties, thermal stability and electrical conductivity, and oxygen storage function [4] [5] [6]. It has been also used in industrial catalysts, solid oxide fuel cells, insulators, UV blockers, gas sensors, high-temperature oxidation resistance, free-radical scavengers, and chemical mechanical polishing (CMP). In addition, cerium oxide (CeO₂) has attracted substantial interest due to its wide band gap for bulk cerium oxide (3.15 - 3.20 eV) semiconductors with light absorption in the UV/Vis region [7].

Additionally, CeO₂ can be blended with other metals or metal oxides to further improve the product performance [2] [3]. However, most of the applications require well-dispersed particles since the aggregated particles lead to inhomogeneous mixing and poor sinterability. Recently, cerium oxide nanoparticles have been found to mitigate oxidative stress damage, such as Parkinson's and Alzheimer's diseases [4]. In addition, cerium oxide was a stronger anticancer material, leading to a reduction of tumor mass in vivo [8]. The antioxidant activities are dependent on the method of synthesis. However, several methods have been reported in the literature, such as the co-precipitation method [2] [9], hydrothermal method [10], sonochemical method [11] [12], sol-gel method [5], micro-emulsion method, and spray-pyrolysis method [13]. Using different cerium ions sources, Hsu *et al.* [14] prepared cerium oxide by the precipitation method and found that the pH value affected the particle morphology. The pH value that affected the precipitation of cerium oxide was also found by Ramachandran *et al.* [15]. Using Ce(NO₃)₃·6H₂O with different precipitation agents, the well-dispersed powders of cerium oxide can be obtained [16]. Zhang *et al.* [17] found that Ce³⁺ concentration, ultrasonic wave, and dispersant agents have significant effects on the crystal size of cerium oxide. Zhou *et al.* [18] mixed the cerium nitrate and ammonium water into a hydrothermal reactor to prepare cerium oxide; they obtained dozens of cerium oxide nanometers with good crystallinity. Increasing the thermal reaction temperature to 400°C (critical state), using water as a critical fluid could modify the growth direction of crystals [18]. Using the sonochemical method [11], the additives affected the particle size and particle size distribution, and a blue shift from UV spectra analysis was observed. Kirk *et al.* [19] used the sol-gel method to prepare cerium oxide and found that crystal densification phenomena increased with calcination temperature and that the calcination temperature had an effect on the growth rate of crystal surface, especially for (111) surface. In addition, the effect of cobalt ion and different solvents on the lattice parameters was to be found by Arul *et al.* [6] and Sakthiraj and Karthikeyan [5], respectively. Therefore, the increase in lattice expansion in a lattice can be used to monitor the particle size and activity of cerium oxide [6]. In addition, some researchers also studied the effect of cobalt

doping on the structural, optical, and redox properties of cerium oxide nanoparticles [20] [21]. The cobalt ion doping concentration was in the range of 1 - 7 mol%. They found that the crystal sizes and energy gaps both decreased with an increase in cobalt ion concentration. A shift in the absorption towards a longer wavelength was observed for Co ion-doped CeO₂.

Regarding the precipitation method, the formation mechanism of cerium oxide was suggested below [7]:



A two-step process for preparing cerium oxide was presented. It involved the formation of cerium hydroxide with hydration reaction and then cerium oxide was obtained with a dewatering process.

From the above literature survey, we found that the crystal size and energy gap measurements were significant in applications. Due to this, the crystal sizes are measured by XRD with the Scherer equation [2] [17] and Williamson-Hall (W-H) method [7]. The Scherer equation is:

$$d_p = \frac{k\lambda}{B \cos \theta} \quad (3)$$

Here, k is the shape factor (=0.9), B is the line broadening at half the maximum intensity (FWHM) in radians, λ is the wavelength of X-ray (0.1542 nm) and θ is the Bragg diffraction angle. The W-H equation is:

$$B \cos \theta = \frac{k\lambda}{d_p} + 4\varepsilon \sin \theta \quad (4)$$

In Equation (4), the crystal size can be determined by using a plot of $B \cos \theta$ versus $4 \sin \theta$. On the other hand, the energy gaps were calculated using absorption coefficient (α) and frequency (ν) [2] [19]. The equation is:

$$\alpha(h\nu) = A(h\nu - E_g)^{1/2} \quad (5)$$

Here, A is constant and E_g is the energy gap. The energy gaps of cerium oxide were found to be 3.26 eV (380 nm) and 3.22 eV (385 nm) [2], while the energy gaps for different solvents [19] were 3.44 eV (361 nm), 3.22 eV (386 nm), 3.45 eV (361 nm) and 3.2 eV (388 nm) for water, acetone, ethanol, and ethylene glycol, respectively. Alternatively, the energy gap can be evaluated by the following equation [22]:

$$E_g (\text{eV}) = \frac{1240}{\lambda_g (\text{nm})} \quad (6)$$

where λ_g is the maximum absorption peak in the UV/Vis spectra. Using Equation (6), the energy gaps reported by Farahmandjou *et al.* [2] and Sakthiraj and Karthikeyan [5] can be calculated and the data shown in **Figure 1**. It was found that the data were close for both. Therefore, Equation (6) was found to be effective to calculate the energy gaps when the maximum absorption peak was given.

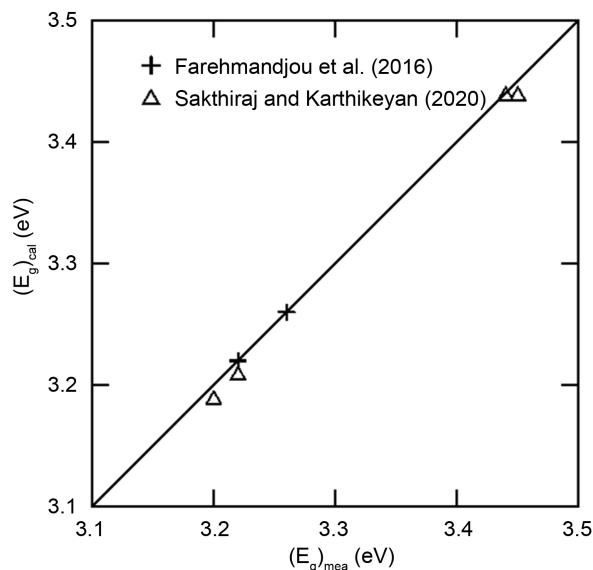


Figure 1. A plot of calculated E_g versus measured E_g shows the confidence of Equation (6).

However, up to now, using the co-precipitation method, only a few papers discussed the effects of cobalt ion at lower concentrations (1 - 7 mol%) and at higher temperatures ($>80^\circ\text{C}$) on crystal size, morphology, and energy gap [20] [21]. Therefore, the purpose of this work was to adapt the co-precipitation method to prepare cerium oxide to explore the effect of operating variables, such as lower temperature ($<80^\circ\text{C}$) and higher concentration of cobalt ion (>16.7 mol%), on the crystal size, morphology, and optical property. Due to this, the operating conditions could be designed. Here, the cerium oxide crystal sizes and energy gaps were evaluated by Equation (3) and Equation (6), respectively. In order to evaluate the reliability of both equations, the results would be compared with that reported in the literature. In addition, the result of the energy gap would be compared with the Brus equation. Finally, the effect of variables on particle size has been discussed and expressed quantitatively in terms of empirical equations.

2. Experimental Feature

Raw materials used were aqueous cerium nitrate ($\text{Ce}(\text{NO}_3)_3 \cdot 6\text{H}_2\text{O}$) solution, aqueous cobalt nitrate ($\text{Co}(\text{NO}_3)_2 \cdot 6\text{H}_2\text{O}$) solution, aqueous ammonia solution, ethanol, and distilled water; all of these were of analytical grade. First, a 0.5 M of cerium nitrate solution (A) and then cobalt nitrate solutions (B) were prepared into desired concentrations. The two solutions were mixed for ten minutes, and then the ammonia solution (28%) was added to the mixed solution and stirred for 20 min. The precipitate was then aged at different temperatures for 24 h and dried in the oven for 24 h. The products were washed several times with distilled water and alcohol, and then the wet cake was placed into the oven and heated at 70°C for 5 h. The dried precipitates were pulverized, and the calcination temperature was determined by TGA (SDT-Q600, TA, USA) before calcination.

Subsequently, dried powders were calcined at the desired temperature (after TGA analysis) for 2 hours at least [21]. Finally, the calcined powders were characterized by X-ray diffraction (XRD) (Rigaku, D/Max-2200/PC, Tokyo, Japan), scanning electron microscope (FESEM) (Jeol, JSM-6500F, Tokyo, Japan), and UV/Vis (Jasco V-670, Tokyo, Japan) instruments for determining the composition, crystal size, morphology and optical property of the precipitates. UV spectrum for cerium oxide can be determined by the Jasco V-670 machine. First, scan the blank in the wavelength range of 200 - 1000 nm by using an integrating sphere (ISN-723). Secondly, put the sample into the measurement cell (radius 1.5 cm, thickness 1.0 mm) and scan the samples in the wavelength range of 200 - 1000 nm. Finally, the absorption spectrum was obtained. The spectrum was overlapped for comparison. The operating conditions were listed in **Table 1**. To understand the experimental procedure in detail, a procedure sheet was shown in **Figure 2**.

3. Results and Discussion

3.1. Determination of Calcination Temperature by TGA

The amount of 0.015 g of dried precipitate was analyzed by TGA and heated to 1000°C at a rate of 10°C/min. The result in **Figure 3** showed that the weight loss of the sample smoothly decreased with heating time and leveled off at 400°C (about 40 minutes), at which point, CeO₂ was formed gradually; thus, 400°C was selected as the temperature for calcination. The annealed temperature was similar to that reported by Ansari *et al.* [21].

3.2. Crystallization at 25°C

XRD diffraction patterns of cerium oxide at 25°C are shown in **Figure 4** (before calcination, No.A1). **Figure 5** shows that the major XRD peaks after calcinations

Table 1. Operating conditions conducted in this work.

No.	Concentration of cerium nitrate (M)	Concentration of cobalt nitrate (M)	Aging temperature (°C)
A1	0.5	0.1	25
A2	0.5	0.3	25
A3	0.5	0.5	25
B1	0.5	0.1	0
B2	0.5	0.3	0
B3	0.5	0.5	0
C1	0.5	0.1	70
C2	0.5	0.3	70
C3	0.5	0.5	70

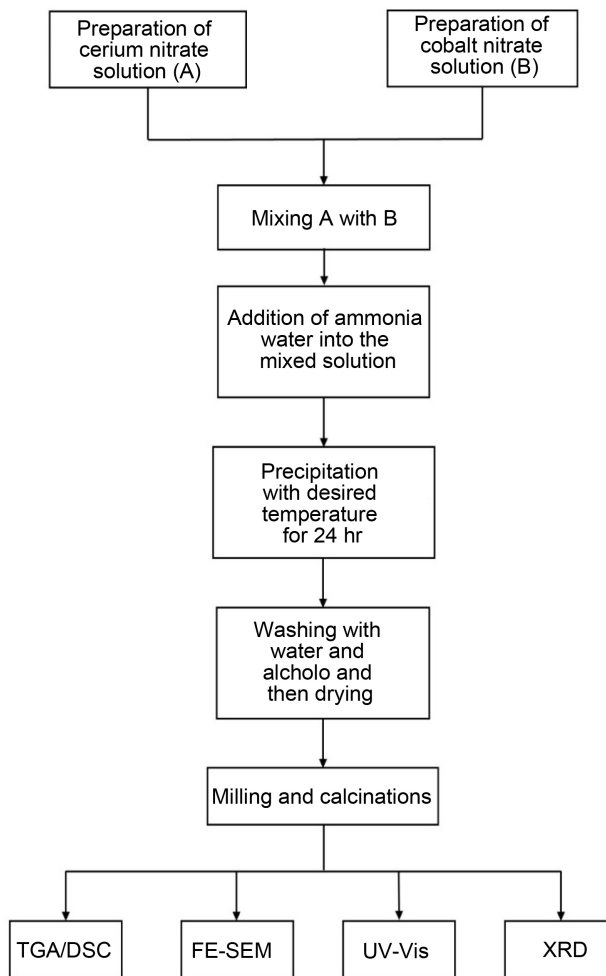


Figure 2. A flow sheet of experimental procedure in this work.

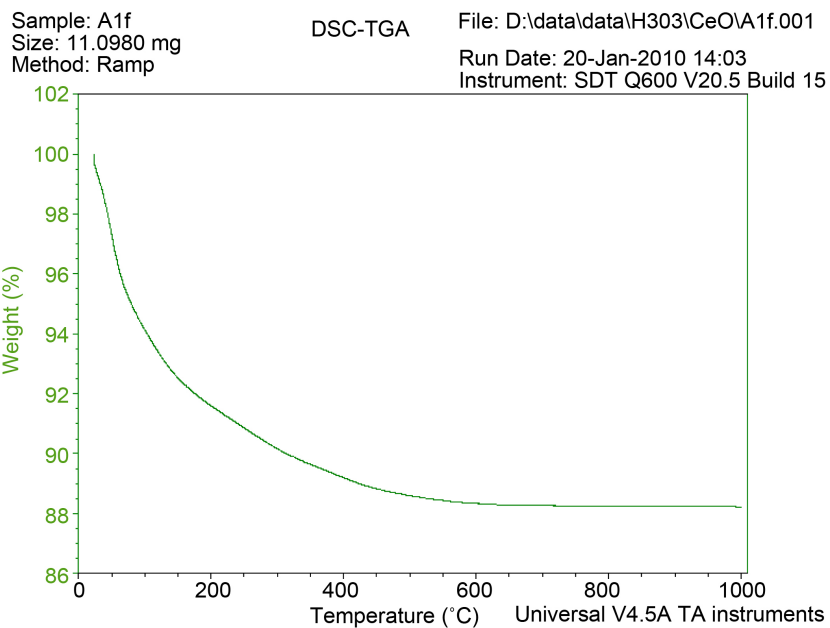


Figure 3. TGA heating process for CeO₂.

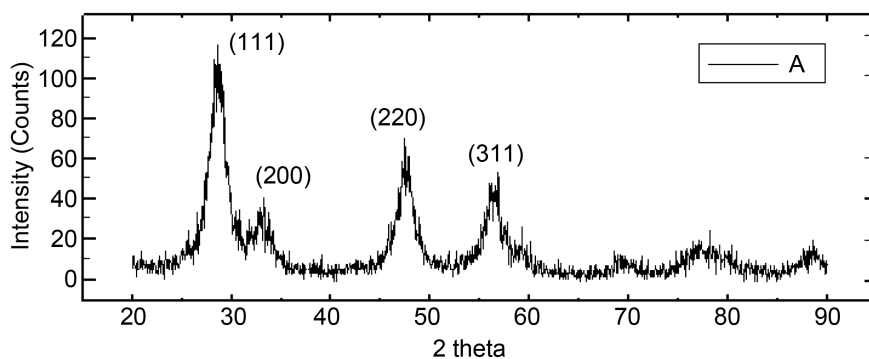


Figure 4. XRD diffraction pattern for No. A1 before calcination.

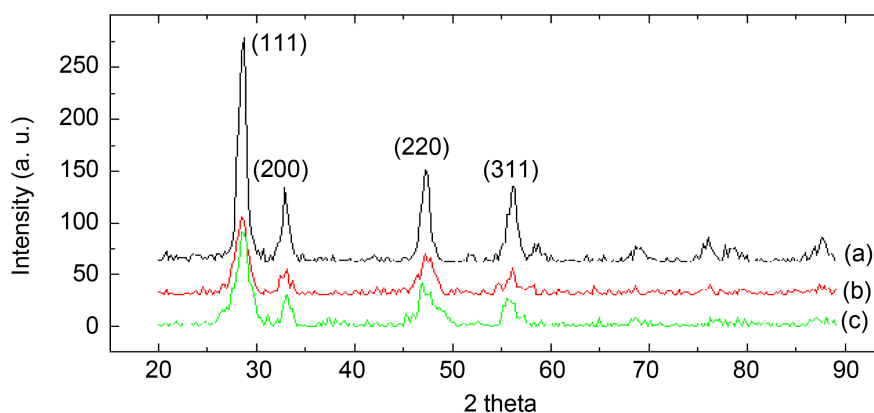
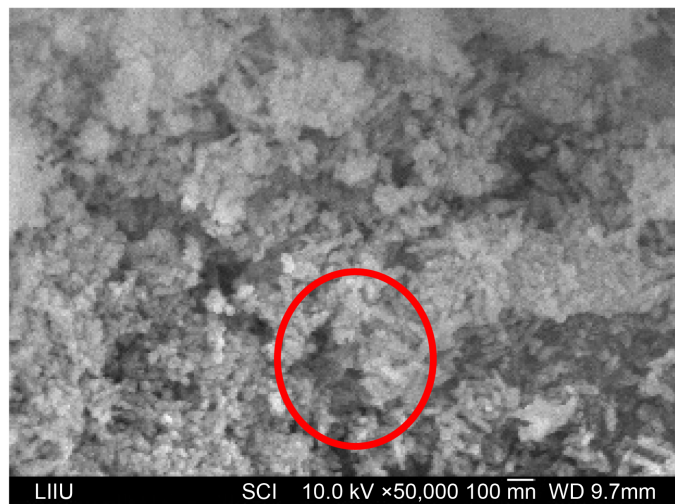


Figure 5. XRD diffraction patterns for series A (25°C) at different cobalt concentrations: (a) 0.1 M (A1), (b) 0.3 M (A2), (c) 0.5 M (A3).

for different cobalt concentrations were at (111), (200), (220) and (311), which were the same as that before calcination. The crystal planes are in accordance with JCPDS No: 34-0394 of cerium oxide crystals [5] [6]. The peak strength was found to be weaker when the cobalt ion concentration increased. From the peak strength (111), using the Scherer equation, the crystal sizes were found to be 13.5 nm, 12.4 nm and 12.3 nm for the cobalt ion concentration of 0.1 M, 0.3 M, and 0.5 M, respectively. **Figure 6** shows the SEM photographs for the three runs. The morphology of cerium oxide was columnar-like for A1 and a mixture of granular and columnar-like for A2 and granular for A3. However, the outlook of the picture for No.A3 was cotton-like containing a lot of tiny particles. The higher the cobalt ion concentration is, the smaller the cerium oxide size is. The possible reason was that the higher cobalt ion concentration decreased the growth rate of cerium oxide resulting smaller size. The UV absorbance (in a.u.) spectrum was shown in **Figure 7**. The highest UV/Vis absorption peak was around 340 nm for all samples, while the absorption curve in the visual region was the lowest for No.A1 without calcination. In addition, the absorption spectra showed that cobalt ion concentration had some effect on the maximum absorption peak. The differences in maximum peaks are found to be 345 nm, 340 nm, 350 nm and 380 nm for (a), (b), (c), and (d), respectively. Besides, the cerium oxide absorbance



(a) 0.1 M (A1)



(b) 0.3 M (A2)



(c) 0.5 M (A3)

Figure 6. SEM photographs of ceria powders for different cobalt concentrations at 25°C (After calcination).

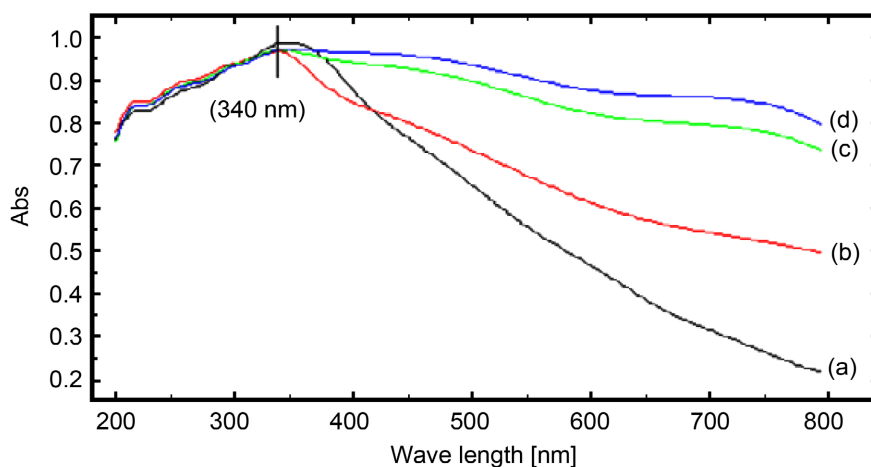


Figure 7. The effect of cobalt ion concentration on the UV/Vis absorption spectra of ceria. (a) No.A1 (before calcination), (b) No.A1 (0.1 M), (c) No.A2 (0.3 M), (d) No.A3 (0.5 M).

curve shown in the visual region became higher when the cobalt ion concentration increased further. From maximum absorption peaks, the energy gaps for four samples can be estimated by Equation (6). The energy gap was found to be 3.59 eV (a), 3.65 eV (b), 3.54 eV (c) and 3.26 eV (d), respectively.

3.3. Crystallization at 0°C

Figure 8 shows the XRD diffraction pattern at 0°C for No. B1 before calcination. The major XRD peaks were also at (111), (200), (220), and (311), which were similar to that shown in **Figure 4**. The XRD peaks after calcination, series B, for different cobalt ion concentration is shown in **Figure 9**. The XRD peaks became weaker as the cobalt ion concentration was increased further. The crystal sizes were found to be 12.7 nm, 12.1 nm, and 11.8 nm for the cobalt ion concentration of 0.1 M, 0.3 M, and 0.5 M, respectively. The sizes were slightly smaller than that conducted at 25°C.

Figure 10 shows the SEM images for the three runs. The morphology of cerium oxide was granular and columnar-like for B1, B2, and B3. However, the outlook of picture for the three pictures was agglomerated with a lot of tiny particles. Furthermore, **Figure 11** shows that the highest UV/Vis absorption peak was around 360 nm for all samples, while the absorption curve in the visual region was the lowest for No.B1 without calcination. However, the differences in absorption peaks were found at 360 nm (a), 350 nm (b), 375 nm (c) and 390 nm (d). The strength of the cerium oxide absorbance curve in the visual light region increased with an increase in cobalt ion concentration. The energy gap for four samples evaluated by Equation (6) was found to be 3.44 eV (a), 3.54 eV (b), 3.30 eV (c) and 3.18 eV (d). This showed the effect of cobalt ion concentration on the optical property of cerium oxide.

3.4. Crystallization at 70°C

Figure 12 was the XRD diffraction pattern at 70°C for No. C1 before calcination.

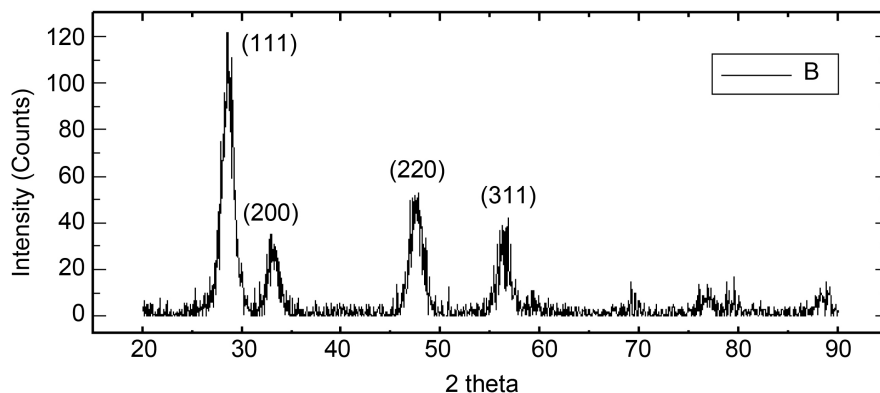


Figure 8. XRD diffraction pattern for No. B1 before calcination.

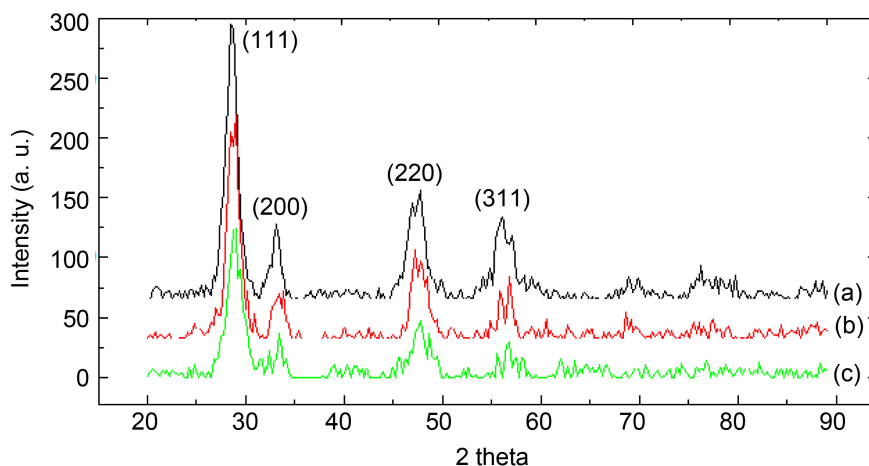
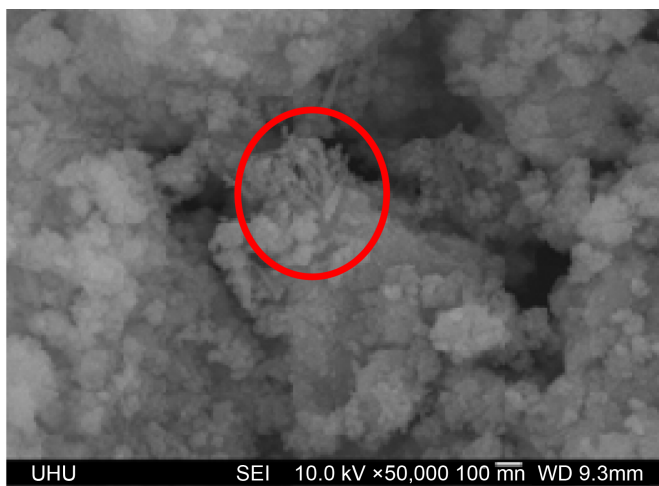


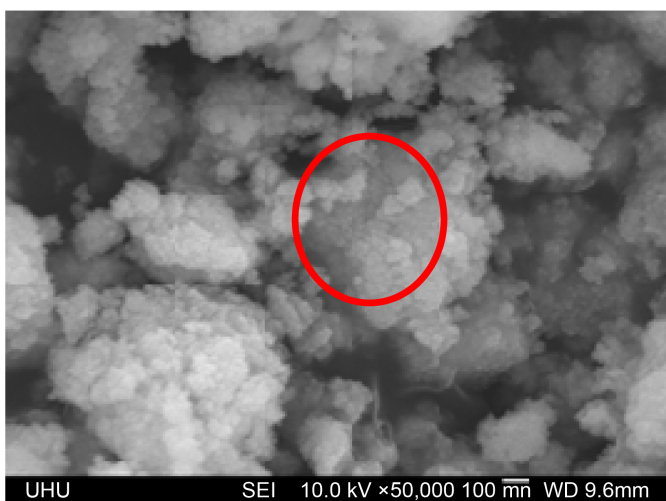
Figure 9. XRD diffraction patterns for series B (0°C) at different cobalt ion concentrations: (a) 0.1 M (B1), (b) 0.3 M (B2), (c) 0.5 M (B3).

The major XRD peaks were also at (111), (200), (220) and (311). However, the peak of (111) was weaker. The XRD peaks after calcination for series C at different cobalt ion concentration is presented in **Figure 13**; the XRD peaks became weaker as the cobalt ion concentration increased further. The crystal sizes evaluated by Equation (3) were found to be 12.60 nm, 12.34 nm, and 12.26 nm for the cobalt ion concentration of 0.1 M, 0.3 M, and 0.5 M, respectively.

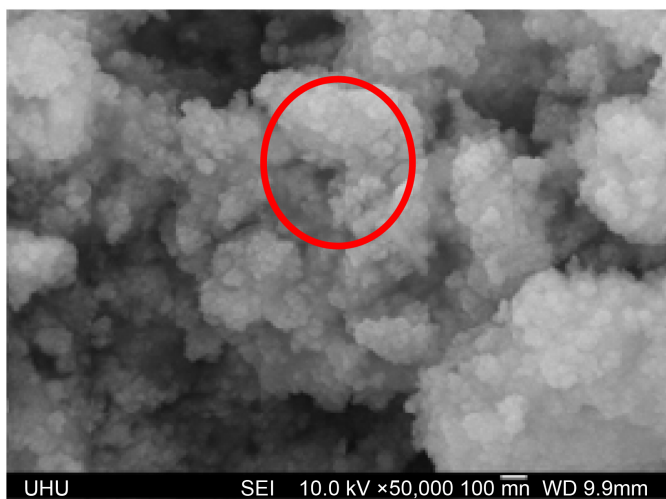
Figure 14 shows the SEM photographs for series C. The morphology of cerium oxide was columnar-like for C1 and C2, while the morphology was granular for C3. However, the pictures for the three runs were all agglomerated with tiny particles. **Figure 15** shows that for all samples, the highest UV/Vis absorption peak was around 334 nm, while the absorption strength in the visual spectra was in the sequence of No. C3 (0.5 M) > No. C2 (0.3 M) > No. C1 (0.1 M). It was found that small differences of maximum peaks were observed, which were found to be 350 nm (a) and 334 nm for (b), (c) and (d), respectively. This illustrated that cobalt ion concentration has no significant effect on the maximum absorption peaks at 70°C. Herein, the energy gaps for four samples estimated by Equation (6) were 3.54 eV (a) and 3.71 eV for (b), (c) and (d).



(a) 0.1 M (B1)



(b) 0.3 M (B2)



(c) 0.5 M (B3)

Figure 10. SEM pictures for series B (0°C) at different cobalt concentrations: (a) 0.1 M (B1), (b) 0.3 M (B2), (c) 0.5 M (B3).

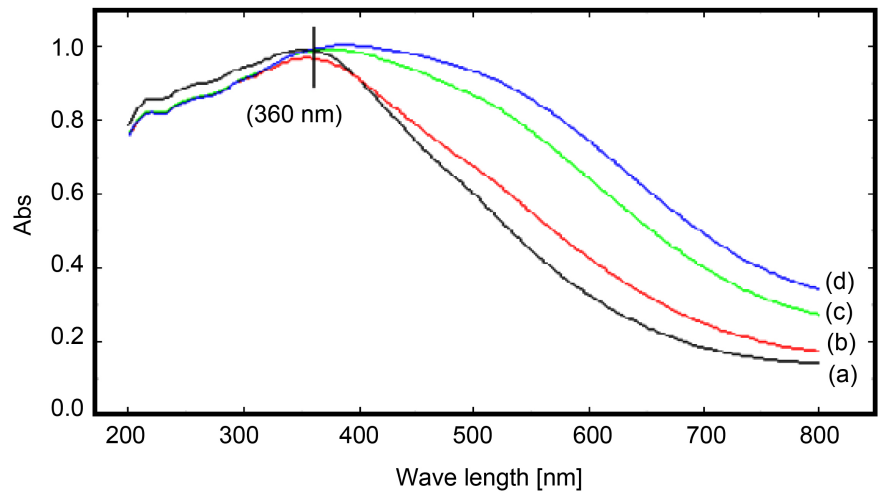


Figure 11. The effect of cobalt ion concentration on the UV/Vis absorption spectra of cerium oxide. (a) No.B1 (before calcination), (b) No.B1 (0.1 M), (c) No.B2 (0.3 M), (d) No.B3 (0.5 M).

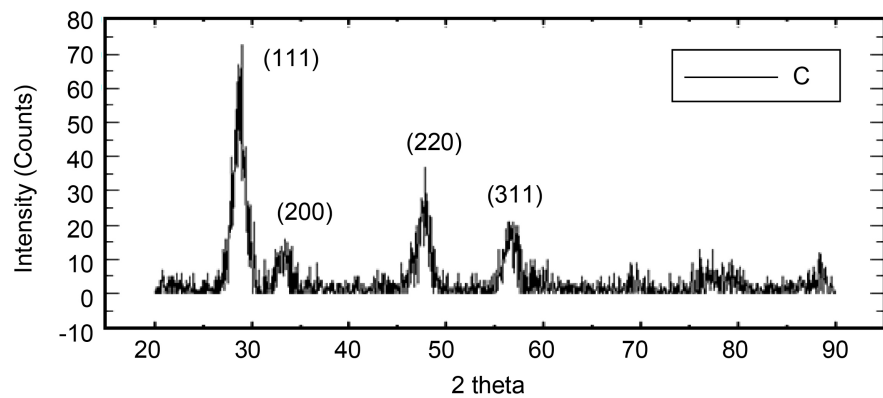


Figure 12. XRD diffraction pattern for No. C1 before calcination.

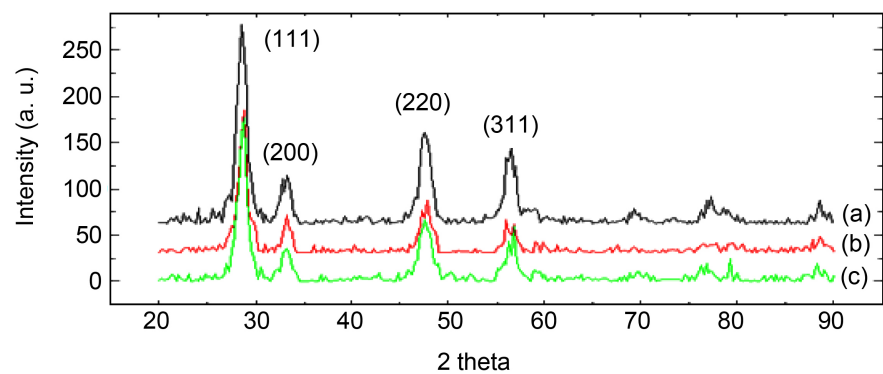
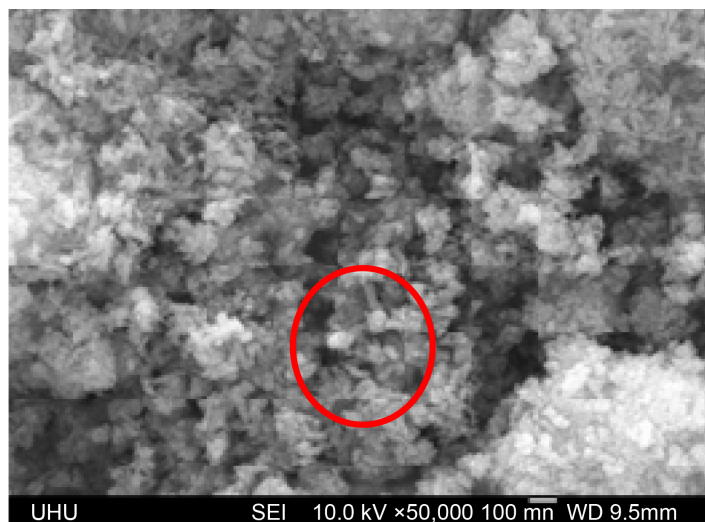


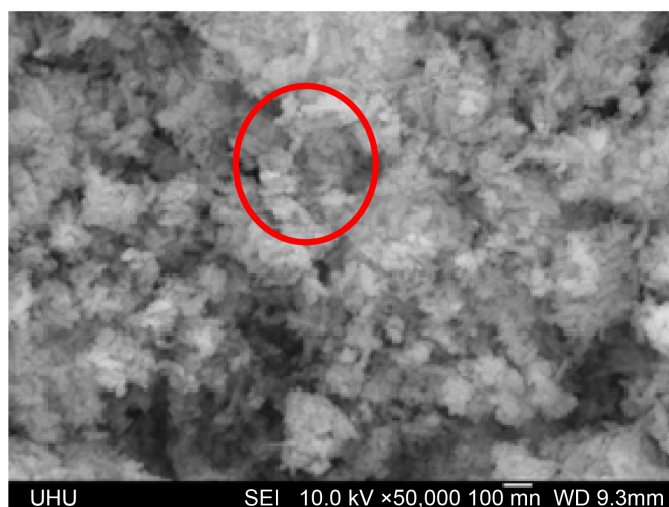
Figure 13. XRD diffraction patterns for series C (70 °C) at different cobalt ion concentrations: (a) 0.1 M (C1), (b) 0.3 M (C2), (c) 0.5 M (C3).

3.5. Comparisons of Crystal Sizes and Energy Gaps

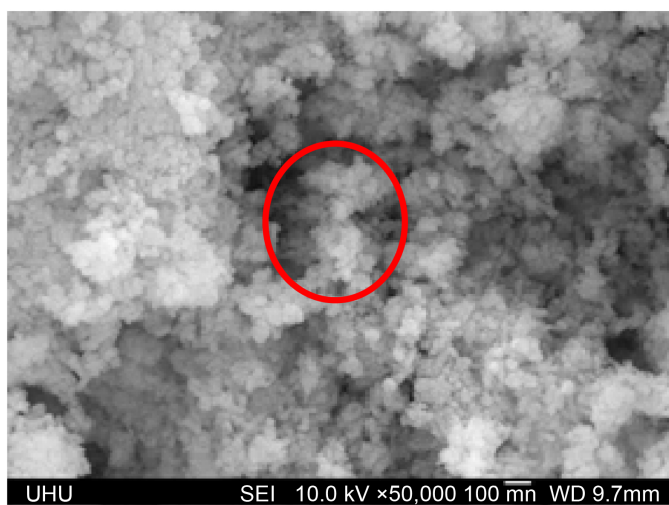
Data collected here were listed in **Table 2**. Crystal sizes obtained from the precipitation method at different temperatures were in the range of 11.82 - 13.47



(a) 0.1 M (C1)



(b) 0.3 M (C2)



(c) 0.5 M (C3)

Figure 14. SEM pictures for series C (70°C) at different cobalt concentrations: (a) 0.1 M (C1), (b) 0.3 M (C2), (c) 0.5 M (C3).

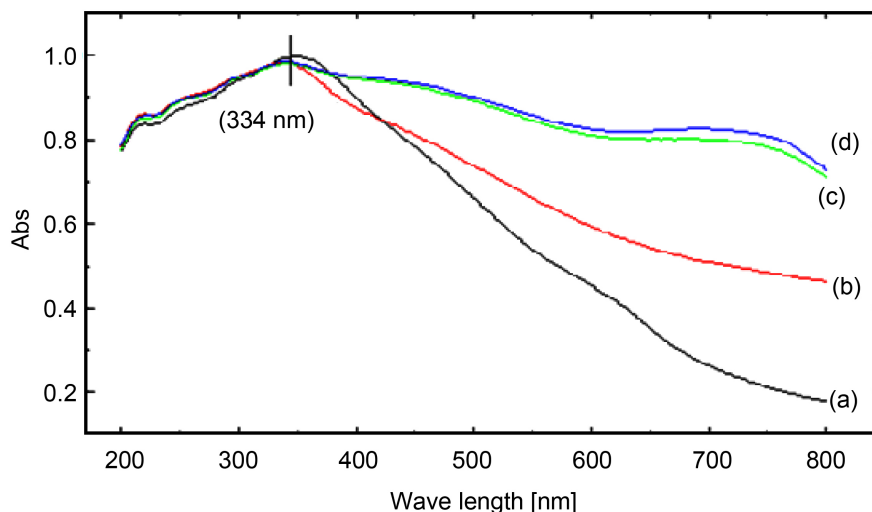


Figure 15. The effect of cobalt ion concentration on the UV/Vis absorption spectra of ceria. (a) No.C1 (before calcination), (b) No.C1 (0.1 M), (c) No.C2 (0.3 M), (d) No.C3 (0.5 M).

Table 2. Data obtained in this work.

No.	[Ce ³⁺] (M)	[Co ²⁺] (M)	<i>T</i> (°C)	Maximum peaks (nm)	Crystal Size (nm)	<i>E_g</i> (eV)
A1	0.5	0.1	25	340	13.47	3.65
A2	0.5	0.3	25	350	12.42	3.54
A3	0.5	0.5	25	380	12.28	3.26
B1	0.5	0.1	0	350	12.66	3.54
B2	0.5	0.3	0	375	12.11	3.30
B3	0.5	0.5	0	390	11.82	3.18
C1	0.5	0.1	70	334	12.60	3.71
C2	0.5	0.3	70	334	12.34	3.71
C3	0.5	0.5	70	334	12.26	3.71

nm. The size range obtained here was comparable with that reported by Farahmandjou *et al.* [2] (20 nm), Arul *et al.* [7] (7 - 12 nm), Corsi *et al.* [8] (10 - 13 nm), Sakthiraj and Karthikeyan [5] (12.0 - 16.3 nm), Chen and Change [21] (7.4 - 16.4 nm), and Chelliah *et al.* [23] (9 - 16 nm). The reports suggest that controlling crystal sizes and morphology depend not only on synthesis methods but also on the operating conditions. In addition, the UV/Vis absorption spectra showed that the maximum peaks were in the range of 334 - 390 nm, indicating a wider maximum absorption peaks range was found by the co-precipitation. The higher the temperature, the smaller the maximum absorption peaks, giving the larger E_g . The corresponding energy gaps were 3.18 - 3.71 eV, while the reported data for E_g were 3.22 - 3.26 eV [2], 3.19 - 3.44 eV [5], and 3.56 - 3.72 eV [24]. Effect of Co ion on the E_g was found in this work. The E_g decreased with an increase in

the Co ions concentration as shown in **Figure 2**. This was due to the addition of Co ions creating oxygen vacancies and favoring the formation of Ce^{3+} from Ce^{4+} , resulting in the formation of localized energy states that are closer to the conduction band, thereby decreasing the E_g [21]. In order to compare with that reported in the literature, crystal sizes and energy gaps for several methods were listed in **Table 3**. The size range and energy gap were found to be in the range of 2.64 - 20 nm and 2.51 - 3.84 eV, respectively. However, the data obtained in this work were comparable with that reported in literatures [2] [5] [20] [21] [24] [25].

3.6. Empirical Equation

To understand the effect of temperature and concentration of cobalt ion on the crystal size for the co-precipitation method, data shown in **Table 2**, a regression of crystal size (d_p in nm) with aging temperature (T in K) and cobalt ion concentration C_B (M) is shown below:

$$d_p = 12.38 \exp\left(-\frac{133.3}{RT}\right) C_B^{-0.03991} \quad (7)$$

The mean root mean error was 0.822% with $R^2 = 0.6325$. The deviation was acceptable. The results in Equation (7) indicate that the particle size decreases with C_B and increased slightly with T . The effect of size on the energy gap was discussed in the next section.

3.7. Energy Gap

The effect of size on the energy gap can be described by Brus equation [25]:

$$E_g = E_{Bulk} + \frac{2h^2\pi^2}{d_p^2} \left[\frac{1}{m_e} + \frac{1}{m_h} \right] - \frac{3.6e^2}{\epsilon_r \epsilon_0 d_p} \quad (8)$$

where E_{bulk} is the bandgap (for CeO_2 ; $E_{bulk} = 3.15$ eV), d_p is the diameter of crystals, m_e and m_h are the effective masses of electron and hole, respectively, and ϵ_r and ϵ_0 are the relative dielectrics constant of CeO_2 , which is 24.5, and dielectric constant at empty, respectively. In here, we use $m_e = m_h = 0.4 m$ where m is the

Table 3. A comparison of crystal size and energy gap for different methods.

Sizes (nm)	E_g (eV)	Methods	References
2.64 - 8.36	3.30 - 3.84	Co-precipitation method	Zhang <i>et al.</i> [25]
20.00	3.22 - 3.26	Co-precipitation method	Farahmandjou <i>et al.</i> [2]
11.99 - 16.30	3.20 - 3.45	Sol-gel method	Sakthiraj and Karthikeyan [5]
7.90 - 16.40	3.56 - 3.71	Co-precipitation method	Chen and Chang [24]
17.04 - 19.94	-	Two-emulsion method	Lee <i>et al.</i> [26]
4.43 - 8.51	2.51 - 2.80	Co-precipitation method	Killivalavan <i>et al.</i> [20]
1.26 - 15.40	2.68 - 2.82	Co-precipitation method	Ansari <i>et al.</i> [21]
11.82 - 13.47	3.18 - 3.71	Co-precipitation method	This work

mass of a free electron. Equation (8) states that E_g is inversely proportional to d_p . The second term and the third term are represented by blue shift and red shift, respectively. In order to compare, the parameters in Equation (8) were listed in **Table 4**. Using the parameters in **Table 4**, the Brus equation can be calculated and expressed as a block dot with a dotted line as shown in **Figure 16**. In addition, the data obtained in this work and from the literature [2] [5] [22] [23] [25] were also presented in this figure. All the data were under the dotted line, which stated that the data evaluated by the Brus equation was overestimated in E_g when d_p was smaller than 20 nm. According to Equation (8), the maximum size (bulk size) can be determined when we let $dE_g/d(d_p) = 0$. The final size was equal to 214 nm, which was the bulk size of cerium oxide. The corresponding E_{bulk} is 3.15 eV.

Table 4. Parameters used in Equation (8).

Parameters	Values
h	$6.63 \times 10^{-34} \text{ m}^2 \cdot \text{kg} \cdot \text{s}^{-1}$
e	$1.60 \times 10^{-19} \text{ C}$
m_e	0.4 m
m_h	0.4 m
m	$9.109 \times 10^{-31} \text{ kg}$
ϵ_r	24.5
ϵ_0	$8.8541 \times 10^{-12} \text{ F} \cdot \text{m}^{-1}$

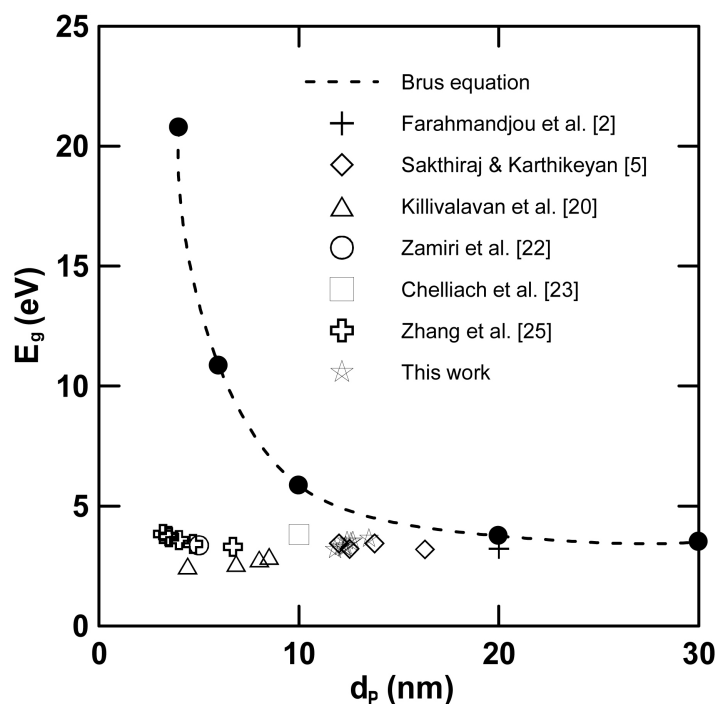


Figure 16. A plot of E_g versus d_p for comparison.

4. Conclusion

In this study, cerium oxide nanoparticles have been successfully prepared by using a co-precipitation process. The effect of higher cobalt ion concentration and lower aging temperature explored in here were found to be an influence on the crystal size, morphology, and energy gap. The mean crystal size of the cerium oxide calculated by the Scherer equation is in the range of 8.05 - 13.47 nm, depending on the operating conditions. A correlation equation for the co-precipitation could be obtained indicating that the crystal size decreased with C_B and increased slightly with aging temperature. According to the FESEM observations, the major morphology was columnar-like and granular forms. From the UV/Vis determination, the maximum absorption peaks at the relative wavelength (λ_g) decreased with an increase in temperature and cobalt ion concentration showing a blue shift as temperature increased, while the effect attenuated at 70°C. Due to the confinement size effect, the energy gap increased with a decrease in crystal size as shown by the Brus equation. However, the energy gap values evaluated were found to be higher when the Brus equation was used, especially when the cerium oxide size was less than 20 nm.

Acknowledgements

The authors acknowledge the financial support of the MOST in Taiwan (MOST-110-2221-E-262-003).

Conflicts of Interest

The author declares no conflicts of interest regarding the publication of this paper.

References

- [1] Nikam, A.V., Prasad, B.L.V. and Kulkarni, A.A. (2018) Wet Chemical Synthesis of Metal Oxide Nanoparticles: A Review. *CrystEngComm*, **35**, 1-17. <https://doi.org/10.1039/C8CE00487K>
- [2] Farahmandjou, M., Zarinkamar, M. and Firoozabadi, T.P. (2016) Synthesis of Cerium Oxide (CeO₂) Nanoparticles Using Simple Co-Precipitation Method. *Revista Mexicana de Física*, **62**, 496-499.
- [3] Bumajdad, A., Eastoe, J. and Mathewa, A. (2009) Cerium Oxide Nanoparticles Prepared in Self-Assembled Systems. *Advances in Colloid and Interface Science*, **147-148**, 56-66. <https://doi.org/10.1016/j.cis.2008.10.004>
- [4] Nyoka, M., Choonara, Y.E., Kumar, P., Kondiah, P.P.D. and Pillay, V. (2020) Synthesis of Cerium Oxide Nanoparticles Using Various Methods: Implications for Biomedical Applications. *Nanomaterials*, **10**, Article No. 242. <https://doi.org/10.3390/nano10020242>
- [5] Sakthiraj, K. and Karthikeyan, B. (2020) Synthesis and Characterization of Cerium Oxide Nanoparticles Using Different Solvents for Electrochemical Applications. *Applied Physics A*, **126**, Article No. 52. <https://doi.org/10.1007/s00339-019-3227-z>
- [6] Arul, N.S., Mangalaraj, D., Chen, P.C., Ponpandian, N. and Viswanathan, C. (2011)

- Self Assembly of Co Doped CeO₂ Microspheres from Nanocubes by Hydrothermal Method and Their Photo Degradation Activity on AO7. *Materials Letters*, **65**, 3320-3322. <https://doi.org/10.1016/j.matlet.2011.07.017>
- [7] Arul, N.S., Mangalaraj, D., Kim, T.W., Chen, P.C., Ponpandian, N., Meena, P. and Masuda, Y. (2012) Synthesis of CeO₂ Nanorods with Improved Photocatalytic Activity: Comparison between Precipitation and Hydrothermal Process. *Journal of Materials Science. Materials in Electronics*, **24**, 1644-1650.
- [8] Corsi, F., Caputo, F., Traversa, E. and Ghibelli, L. (2018) Not Only Redox: The Multifaceted Activity of Cerium Oxide Nanoparticles in Cancer Prevention and Therapy. *Frontiers in Oncology*, **8**, Article No. 309. <https://doi.org/10.3389/fonc.2018.00309>
- [9] Pujar, M.S., Hunagund, S.M., Desai, V.R., Patial, S. and Sidarai, A.H. (2017) One-Step Synthesis and Characterization of Cerium Oxide Nanoparticles in an Ambient Temperature via Co-Precipitation Method. *DAE Solid State Physics Symposium*, Mumbai, 26-30 December 2017, Article ID: 050026. <https://doi.org/10.1063/1.5028657>
- [10] Zhou, Y.C. and Rahaman, M.N. (1993) Hydrothermal Synthesis and Sintering of Ultrafine CeO₂ Powders. *Journal of Materials Research*, **8**, 1680-1686. <https://doi.org/10.1557/JMR.1993.1680>
- [11] Yin, L., Wang, Y., Pang, G., Kolytyn, Y. and Gedanken, A. (2002) Sonochemical-Synthesis of Cerium Oxide Nanoparticles-Effect of Additives and Quantum Size Effect. *Journal of Colloid and Interface Science*, **246**, 78-84. <https://doi.org/10.1006/jcis.2001.8047>
- [12] Yu, J. C., Zhang, L. and Lin, J. (2003) Direct Sonochemical Preparation of High-Surface-Area Nanoporous Ceria and Ceria-Zirconia Solid Solutions. *Journal of Colloid and Interface Science*, **260**, 240-243. [https://doi.org/10.1016/S0021-9797\(02\)00168-6](https://doi.org/10.1016/S0021-9797(02)00168-6)
- [13] Yoshioka, T., Dosaka, K., Sato, T., Okuwaki, A., Tanno, S. and Miura, T. (1992) Preparation of Spherical Ceria-doped Tetragonal Zirconia by the Spray-Pyrolysis Method. *Journal of Materials Science Letters*, **11**, 51-55. <https://doi.org/10.1007/BF00720779>
- [14] Hsu, W.P., Aiken, B. and Matijevic, E. (1988) Preparation and Properties of Monodispersed Colloidal Particles of Lanthanide Compounds: III, Yttrium(III) and Mixed Yttrium(III)/Cerium(III) Systems. *Journal of the American Ceramic Society*, **71**, 845-853. <https://doi.org/10.1111/j.1151-2916.1988.tb07534.x>
- [15] Ramachandran, M., Subadevi, R. and Sivakumar, M. (2018) Role of pH on Synthesis and Characterization of Cerium Oxide (CeO₂) Nano Particles by Modified Co-Precipitation. *Vacuum*, **161**, 220-224. <https://doi.org/10.1016/j.vacuum.2018.12.002>
- [16] Chen, P.L. and Chen, I.W. (1993) Reactive Cerium (IV) Oxide Powders by The Homogeneous Precipitation Method. *Journal of the American Ceramic Society*, **76**, 1577-1583. <https://doi.org/10.1111/j.1151-2916.1993.tb03942.x>
- [17] Zhang, Q., Yang, Z. and Ding, B. (2009) Synthesis of Cerium Oxide Nanoparticles by Precipitation Method. *Materials Science Forum*, **610-613**, 233-238. <https://doi.org/10.4028/www.scientific.net/MSF.610-613.233>
- [18] Zhou, Y.C. and Rahaman, M.N. (1997) Effect of Redox Reaction on the Sintering Behavior of Cerium Oxide. *Acta Materialia*, **45**, 3635-3639. [https://doi.org/10.1016/S1359-6454\(97\)00052-9](https://doi.org/10.1016/S1359-6454(97)00052-9)
- [19] Kirk, N.B. and Wood, J.V. (1995) The Effect of The Calcinations Process on the

- Crystallite Shape of Sol-Gel Cerium Oxide Used for Glass Polishing. *Journal of Materials Science*, **30**, 2171-2175. <https://doi.org/10.1007/BF00353051>
- [20] Killivalavan, G., Sathyaseelan, B., Kavitha, G., Baskarann, I., Senthilnathan, K., Sivakumar, D., Karthikeyan, N., Manikandan, E. and Maaza, M. (2020) Cobalt Metal ion Doped Cerium Oxide (Co-CeO₂) Nanoparticles Effect Enhanced Photocatalytic Activity. *MRS Advances, Materials Research Society*, **5**, 1-13. <https://doi.org/10.1557/adv.2020.296>
- [21] Ansari, A.A., Labis, J., Alam, M., Ramay, S.M., Ahmad, N. and Mahmood, A. (2016) Effect of Cobalt Doping on Structural, Optical and Redox Properties Cerium Oxide Nanoparticles. *Phase Transitions*, **89**, 261-272. <https://doi.org/10.1080/01411594.2015.1116532>
- [22] Zamiri, R., Ahangar, H.A., Kaushal, A., Zakaria, A., Zamiri, G., Tobaldi, D. and Ferreira, J.M.F. (2015) Dielectrical Properties of CeO₂ Nanoparticles at Different Temperatures. *PLoS ONE*, **10**, e0122989. <https://doi.org/10.1371/journal.pone.0122989>
- [23] Chelliah, M., Rayappan, J.B. and Krishnan, U.M. (2012) Synthesis and Characterization of Cerium Oxide Nanoparticles by Hydroxide Mediated Approach. *Journal of Applied Sciences*, **12**, 1734-1737. <https://doi.org/10.3923/jas.2012.1734.1737>
- [24] Chen, H.I. and Chang, H.Y. (2005) Synthesis of Nanocrystalline Cerium Oxide Particles by the Precipitation Method. *Ceramics International*, **31**, 795-802. <https://doi.org/10.1016/j.ceramint.2004.09.006>
- [25] Zhang, F., Jin, Q. and Chan, S.W. (2004) Ceria Nanoparticles: Size, Size Distribution, and Shape. *Journal of Applied Physics*, **95**, 4319-4326. <https://doi.org/10.1063/1.1667251>
- [26] Lee, J.S., Lee, J.S. and Choi, S.C. (2005) Synthesis of Nano-Sized Ceria Powders by Two-Emulsion Method Using Sodium Hydroxide. *Materials Letters*, **59**, 395-398. <https://doi.org/10.1016/j.matlet.2004.09.033>